Numerical investigation of electronic wave functions in quasiperiodic lattices

1998 J. Phys.: Condens. Matter 10 783

(http://iopscience.iop.org/0953-8984/10/4/008)

J. Phys.: Condens. Matter **10** (1998) 783–800. Printed in the UK PII: S0953-8984(98)80629-2

Numerical investigation of electronic wave functions in quasiperiodic lattices

Thomas Rieth and Michael Schreiber

Institut für Physik, Technische Universität Chemnitz, D-09107 Chemnitz, Germany

Received 3 January 1997, in final form 29 October 1997

Abstract. We study the electronic eigenstates on two- and three-dimensional quasiperiodic lattices using a tight-binding Hamiltonian in the vertex model. In particular, we analyse how a quasiperiodic lattice influences the decay form and the self-similar structure of the wave functions. The investigation of the earlier-suggested power-law localization is performed by calculating participation numbers and the structural entropy of the wave function. We also present results for the multifractal analysis of the eigenstates by a standard box-counting method. The eigenstates of the two-dimensional Penrose lattice display multifractal character. In contrast, most eigenstates of the three-dimensional Amman–Kramer lattice are shown to be extended; localized states occur only in the band tails, where the spectrum appears to be fractal.

1. Introduction

Numerical investigations of the electronic eigenstates on the Fibonacci lattice, a 1D correspondence of quasicrystals [1], suggest that all of the eigenstates are critical, i.e. neither extended all over the lattice as are the Bloch states, nor exponentially localized as are, e.g. the strongly localized states in the Anderson model of localization. It was further shown [2] that the decay of the envelope of the wave function follows a power law and the wave function itself possesses a multifractal structure. The critical character of these wave functions has been related to the competition of the absence of periodicity, which leads to localized wave functions, and the repetitiveness due to Conway's theorem, which causes resonances between equivalent local configurations. Conway's theorem [3] states that in a quasicrystal a given local pattern in a region of some diameter l will be repeated within a distance of two diameters $2l$.

Studies of the electronic structure of 2D and 3D quasiperiodic lattices are usually based on a tight-binding model. Various lattices can be derived from a tiling with fat and thin rhombuses [3] in 2D for the Penrose lattice (PL), or oblate and prolate rhombohedra [4] in 3D, giving the so-called Amman–Kramer lattice (AKL). In the case of the vertex (centre) model, atomic orbitals are placed on the vertices (in the centre) of each rhombus or rhombohedron and an electron is allowed to hop between neighbouring orbitals. Using a real-space renormalization-group theory it was argued [5, 6] that in all quasiperiodic lattices which fulfil Conway's theorem the wave functions should show a power-law localization.

For the Penrose lattice (PL) similar results have been obtained numerically [7–10], but mathematically rigorous results are only available for some exact eigenstates located at particular energies.

First, it is known that in the thermodynamic limit the nearest-neighbour tight-binding models have degenerate eigenstates, called confined states and string states [9, 11–14]. These

0953-8984/98/040783+18$19.50

are strongly localized and their degeneracy is due to Conway's theorem. But they are not really a characteristic property of quasicrystals in themselves, since they are a consequence of the special local topology [9, 14]. Similar spatially confined states and string states have been found also in the AKL [15].

In the vertex model of the PL, a theory [9] based on frustration ideas for a renormalized lattice predicts a change in the nature of the localization properties. It is supposed to change from delocalized states above a certain energy to fractal states below that energy which are localized in specific regions in order to reduce frustration due to amplitude variations [9]. However, in the PL a finite gap separates the spatially confined states in the band centre from the remaining states [9, 14]. Moreover, the existence of the confined states strongly depends on the Hamiltonian. Therefore it may be an oversimplification to conclude that other wave functions have the same character.

The second rigorous result is that one can construct a tight-binding Hamiltonian so that certain multifractal wave functions become its eigenstates by setting long-range transfer energies according to a complex rule [16]. This procedure can be applied to an infinite number of multifractal wave functions, but since this procedure is quite artificial, it is not clear whether multifractal eigenfunctions exist in other simple models, such as nearest-neighbour hopping models. Using the vertex model, Sutherland [17] derived an indexing rule for the vertices by defining two kinds of vector field on a PL. Then, by appropriately choosing the on-site potentials at the vertices the exact self-similar ground-state wave function could be obtained, showing critical, non-normalizable, and multifractal properties.

In the AKL, much less is known than in the PL about spatially confined and about multifractal states. It is our aim to characterize electronic states in the PL and the AKL by means of the participation ratio and the singularity spectrum. These concepts have been extensively applied in the study of the localization behaviour of electronic states in disordered systems described by the Anderson model of localization [18, 19, 27, 28].

In a recent paper [10] we have shown, by numerical investigation of the localization properties for the electronic eigenstates in the vertex model of the PL and the AKL, that the underlying quasiperiodic lattice causes a localization of comparable strength to that due to the weak disorder in the Anderson model [18] but with a different effect on the various eigenstates in the PL. As in the Anderson model, the influence decreases on changing from two to three dimensions. Most of the states in the AKL do not show localization but rather the behaviour of extended states. The purpose of the present paper is to investigate the decay form and the possibility of a multifractal structure of the wave function in the PL and AKL.

2. The model

The construction of the quasiperiodic lattices is based on the grid method described by de Bruijn [20]. In order to be able to apply periodic boundary conditions, we approximate the golden mean $\tau = (\sqrt{5}+1)/2$ by the ratio of two subsequent Fibonacci numbers $F_0 = 0$, $F_1 = 1$ and $F_{n+1} = F_n + F_{n-1}$ with $\lim_{n\to\infty}(F_{n+1}/F_n) = \lim_{n\to\infty}\tau_n = \tau$. Then the matching rules of the PL are violated only for two edges [7]. The system sizes of various periodic approximants which can be constructed in this way are presented in table 1. The resulting unit cell is a fat rhombus in 2D and a cube in 3D.

We use the so-called vertex model together with a tight-binding Hamiltonian. In this model an s orbital is placed at every corner (vertex) of a rhombus or rhombohedron and

only transfer integrals along the edges (bonds) are considered:

$$H = \sum_k |k\rangle \varepsilon_k \langle k| + \sum_{k,m} |k\rangle V_{km} \langle m|. \tag{1}$$

Here the site energies are chosen as $\varepsilon_k = 0$, and the nearest-neighbour transfer integrals or hopping matrix elements are $V_{km} = 1$ for all pairs of vertices connected by a bond and $V_{km} = 0$ otherwise. In the Anderson model of localization, disorder is introduced into the Hamiltonian (1) by randomizing the site energies ε_k. We have investigated [21] the influence of such an energetic disorder on the localization properties of the AKL and found that already a relatively weak disorder deletes all characteristics of the quasicrystals in comparison with square or simple cubic lattices. In the present paper we use vanishingly small disorder for numerical simplification only (see below), and we compare our results concerning the localization behaviour of the electronic states in the quasicrystals with the respective results for energetically disordered square and simple cubic lattices.

Table 1. The number of lattice sites N for the various periodic approximants (F_{n+1}, F_n) of the PL and the AKL.

n	(F_{n+1}, F_n)	N (PL)	N (AKL)
0	(1, 0)	4	8
1	(1, 1)	11	32
2	(2, 1)	29	136
3	(3, 2)	76	576
4	(5, 3)	199	2440
5	(8, 5)	521	10 336
6	(13, 8)	1364	43 784
7	(21, 13)	3571	185 472
8	(34, 21)	9349	
9	(55, 34)	24 476	
10	(89, 55)	64 079	
11	(144, 89)	167 761	

We employ the Householder method for a direct numerical diagonalization of the Hamiltonian for the computation of the eigenstates in lattices with less than $N = 11\,000$ sites, and the Lanczos algorithm [22] for bigger systems. The Lanczos algorithm is especially suited for large sparse matrices as given by the Hamiltonian above. In order to simplify the use of the Lanczos algorithm, the site energies ε_k in equation (1) were chosen at random from a box distribution of very small width, $W = 10^{-5}$. By this trick we avoid numerical degeneracies. Such a small energetic disorder has visible effects only on the degenerate states in the band centre for which the degeneracy is lifted and the confined states appear in a straightforward way. A detailed explanation can be found in our recent article [14].

In figures 1 and 2 two eigenstates in the largest investigated periodic approximant $(F_{n+1}, F_n) = (144, 89)$ of the PL are presented to allow us to visualize examples of the multifractal states proposed for quasiperiodic lattices of dimension $D > 1$ [5, 6]. The figures demonstrate the curdling of the wave functions which is a characteristic feature of multifractal entities: clusters and voids of all sizes occur. In figure 1 regular ring structures can be found repeatedly. But it must be stressed that these are not confined states, because all of these rings belong to one single eigenstate. In figure 2 the probability density is more evenly distributed; the quasicrystalline symmetry of the underlying lattice is much less obvious than in figure 1. Nevertheless the curdling is clear also in this case, but a larger

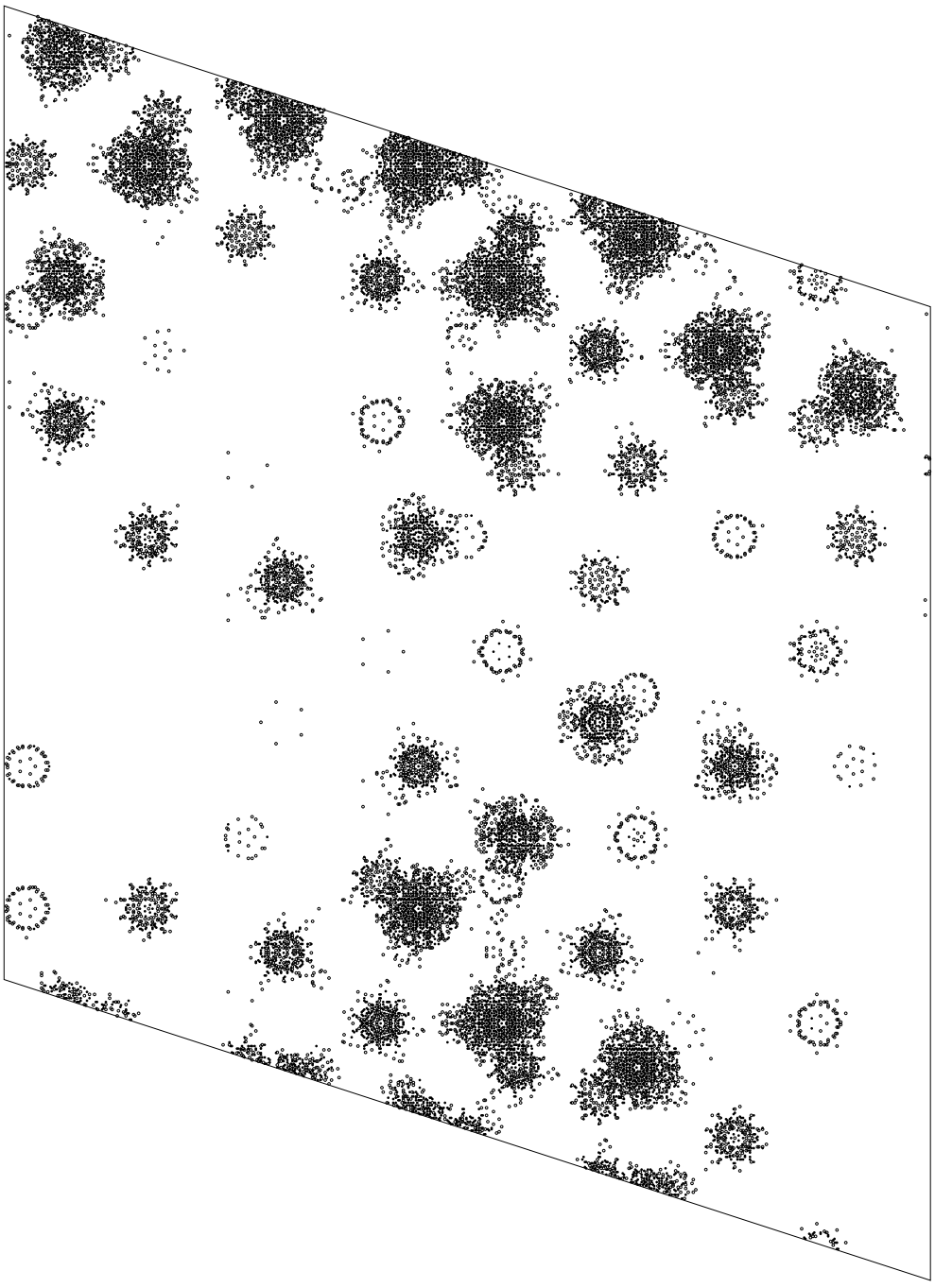

Figure 1. The probability density ρ of an eigenstate at an energy $E = 0.171$ in the periodic approximant $(144, 89)$ of a PL with small energetic disorder, $W = 10^{-5}$. Every site with probability density larger than average is indicated by a circle. For empty circles the density is $\rho > 1/N$ and for filled ones $\rho > 2/N$.

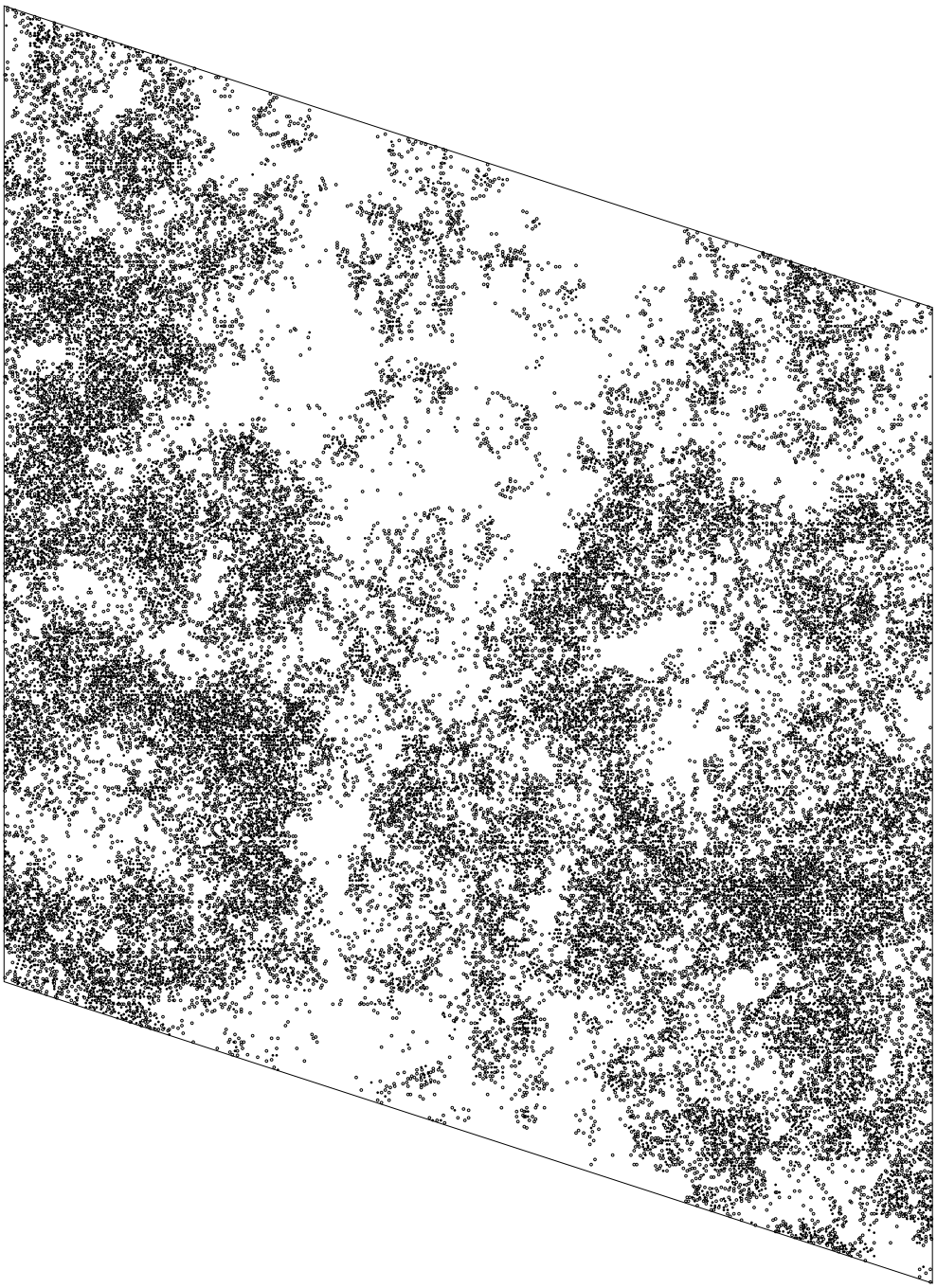

Figure 2. The probability density ρ of an eigenstate at an energy $E = 0.901$ in the periodic approximant $(144, 89)$ of a PL with small energetic disorder, $W = 10^{-5}$. Every site with probability density larger than average is indicated by a circle. For empty circles the density is $\rho > 1/N$ and for filled ones $\rho > 2/N$.

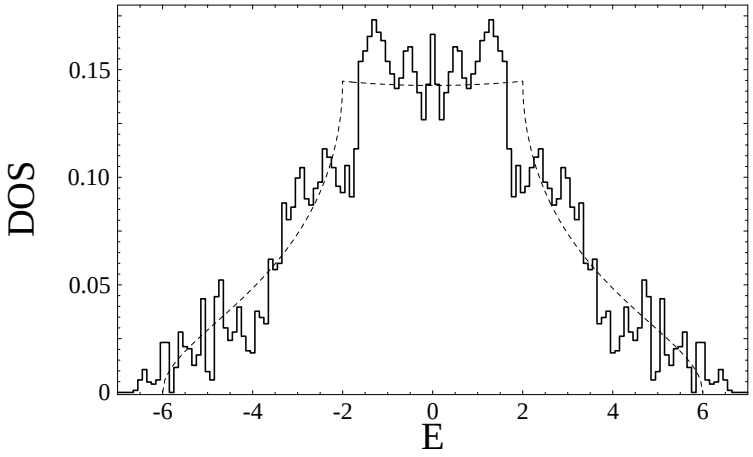

Figure 3. A histogram of the DOS of the approximant (8, 5) of the AKL. For comparison the DOS of a simple cubic lattice is shown by a dashed line.

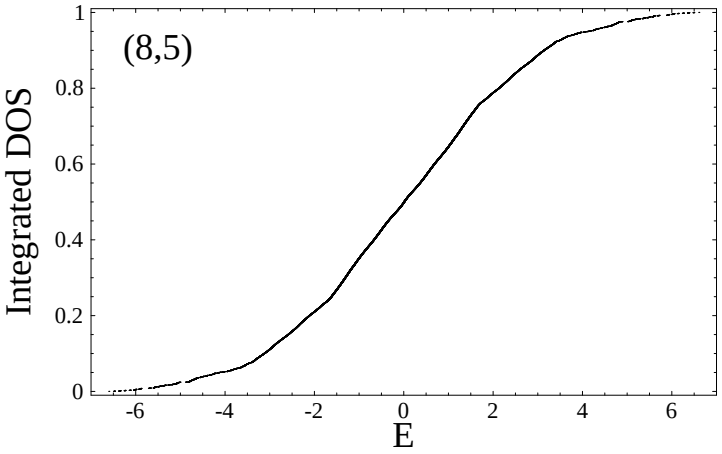

Figure 4. The integrated DOS of the approximant (8, 5) of the AKL.

value of the respective fractal dimensions can be expected. Of course, the multifractality cannot be concluded from a visual inspection of these pictures, but multifractality is already suggested by these plots, which are very similar to the respective plots for Anderson-localized wave functions [27–29]. A detailed quantitative analysis which is necessary to determine the multifractal properties will be presented in section 5.

3. The density of states of the AKL

To get an overview over the properties of the quasicrystalline lattices investigated, we have first determined the density of states (DOS) for the larger approximants. As the DOS of the vertex model of the PL with its characteristic band-centre peak, which is due to the degenerate confined states and separated from the rest of the spectrum by a finite gap, is well known, we do not present our results for the PL here.

The DOS of the AKL in figure 3 shows three different regimes: a broad maximum around the centre, distinct shoulders in the energy range $\pm E \in (1.7, 3.4)$ and a tail in which distinct gaps occur which are not all distinguishable in the histogram of figure 3. Overall, the shape of the DOS is rather similar to the DOS of the simple cubic lattice as indicated in figure 3. A comparison with the DOS of the smaller approximants (not shown here) allows us to conclude that the DOS becomes smoother in the band centre and around the shoulders with increasing size of the approximants. We note that in contrast to the 9.8% degenerate states of the PL, only very few degenerate states occur in the AKL. We have found two degenerate states in the approximant $(5, 3)$ and six in the approximant $(8, 5)$ at $E = 0$. In contrast to the PL, in the AKL the degenerate states are not separated from the rest of the spectrum by a finite gap.

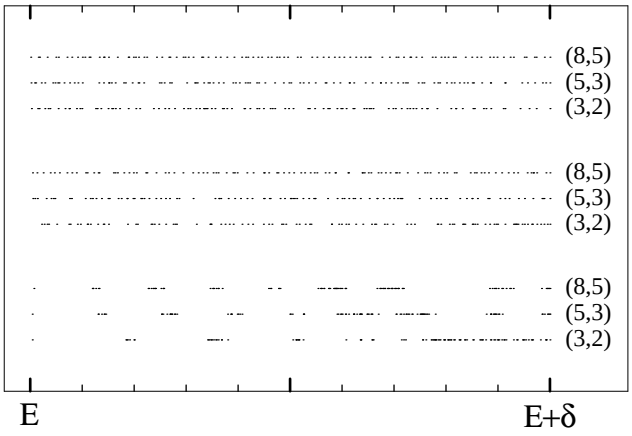

Figure 5. The eigenvalue spectrum of various approximants of the AKL in the centre (top), the shoulders (middle), and the tails (bottom) of the DOS. In each case 100 eigenvalues are indicated in the energy ranges beginning at $E = -1.2, -3.0$ and -6.6, respectively. The interval width δ is adjusted so that the average density is the same in each case. Specifically, from top to bottom, $\delta = 0.06, 0.24, 1.09$, and $0.09, 0.46, 1.65$, and $1.0, 2.3, 4.2$.

Due to the relatively small number of states, it is not appropriate to reduce the width of the bins of the histogram in figure 3 further, so a detailed analysis of possible gaps in the spectrum is difficult. Therefore, in figure 4 we present the respective integrated DOS in which the band-centre regime and the shoulders can be distinguished due to the varying steepness of the curve. In the tails a close inspection reveals indeed several gaps. In order to investigate the changes of the spectrum in the hierarchy of the approximants, in figure 5 we plot parts of the spectrum in the three regimes distinguished. In order to compensate the effect of the significantly different densities for the different approximants, we have chosen different energy scales for the different approximants. (Using the same energy scale, we obtain very large gaps for the smaller approximants; the positioning of these gaps is not retained in any obvious characteristic way in the larger approximant.) In the band centre the spectrum in figure 5 shows a rather homogeneous behaviour already for the smaller approximants. In the shoulder regime the smaller approximants display gaps in the spectrum, which, however, are filled with increasing size of the approximants. In this regime, it appears probable that the spectrum becomes even more homogeneous for larger system size. In contrast, the gaps in the tail region appear to survive even in the larger approximants, although the gap size decreases according to the increasing DOS. Here the

spectrum appears to be fractal. Unfortunately, the system sizes investigated are too small to allow a more detailed analysis and investigation of the question of whether the spectrum in this energy range is singular continuous and whether the eigenstates are critical. From the present data we can only conclude that a characteristic change occurs around $\pm E = 3.4$ in the spectrum. A more detailed analysis based on extensive large-scale computations is planned for the future.

4. Power-law localization

4.1. Participation numbers

To study the localization properties of an eigenstate $|\Psi_j\rangle = \sum_n \psi_{nj}|n\rangle$ of the Hamiltonian (1) we determine the mean fourth power of the amplitude of the wave function [18] in site representation:

$$P^{-1}(E_j) = \int \mathrm{d}^D r \ |\Psi_j(r)|^4 = \sum_{n=1}^{N} \psi_{nj}^4. \tag{2}$$

P is called participation number because it is a measure of the number of sites that contribute significantly to a state of given eigenenergy E_j. The corresponding fraction $p = P/N$ of all of the states is called the participation ratio. For the approximant (8, 5) of the AKL the participation ratios are shown in figure 6. The three different regimes discussed for the DOS can be identified in figure 6 as well. In the centre and in the shoulders of the DOS the participation ratios of various eigenstates do not differ very much. Only small statistical fluctuations occur, except at $E = 0$ where some rather small values of p are found which correspond to the above-mentioned confined states. In the tails of the DOS larger fluctuations can be observed; on average the values of the participation ratio are smaller than in the band centre. The states appear to be grouped at certain energies with a distinct spread of the participation numbers within the groups. The gaps found in the DOS can also be identified here. A comparison with the respective plots for other approximants did not yield more information, because the system sizes are too small to allow definite conclusions to be reached for the individual eigenstates as discussed above.

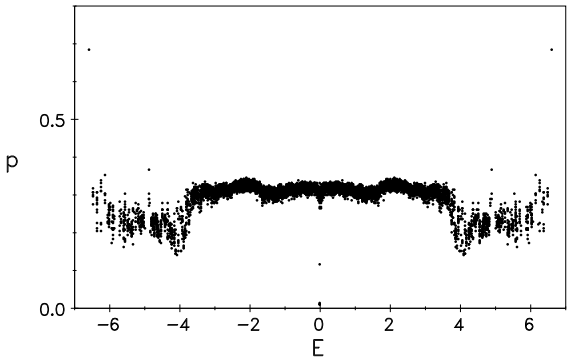

Figure 6. The participation ratio $p = P/N$ of all of the states of the approximant (8, 5) of the AKL, determined by the Lanczos algorithm for a disorder $W = 0.002$. Note the data point at $\pm E_{max} = 6.6$ with $p_{max} = 0.685$.

On averaging the results within a small energy interval, however, a more quantitative analysis of the participation numbers is possible. It is based on the power β of the

dependence of the participation number on the system size:

$$P \propto N^{\beta} \tag{3}$$

which can be used to characterize the localization behaviour of the states. β vanishes for localized states once they fit into a sample of a given size, while $\beta = 1$ for states uniformly extended over the whole sample. In order to explain the proportionality (3) for other values of β one can assume that the wave function or rather its envelope falls off as an inverse power of the distance $\Psi(r) \propto r^{-\alpha}$. Normalizing these wave functions on a finite sample of size $N = L^D$ we get

$$P^{-1} = \left(\int_{\epsilon}^{L} \mathrm{d}r\ r^{D-1}\Psi^4 + C_1\right) \Big/ \left(\int_{\epsilon}^{L} \mathrm{d}r\ r^{D-1}\Psi^2 + C_2\right)^2 \propto \frac{L^{D-4\alpha} + C_1'}{(L^{D-2\alpha} + C_2')^2} \tag{4}$$

where the constants C contain the contributions of some small volume ϵ^D at the origin where Ψ formally diverges. This volume does not characterize the localization behaviour. Taking exponents in the range $D/4 < \alpha < D/2$ we obtain for large L

$$P \propto L^{2D-4\alpha} \qquad \text{or} \qquad \beta = 2 - 4\frac{\alpha}{D}. \tag{5}$$

For smaller values of α the wave function Ψ is not normalizable; for larger values of α the wave function appears so strongly localized that $P \approx$ constant and $\beta = 0$.

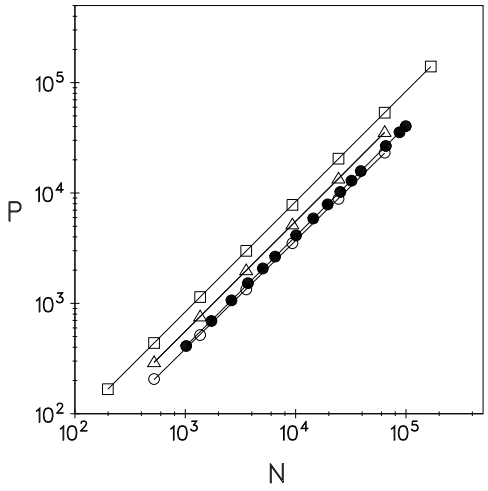

Figure 7. The participation number P versus system size N for the eigenstate of the lowest energy $E = -4.234$ in the PL. The values are calculated for periodic approximants with periodic (□), antiperiodic (△) and open (○) boundary conditions, and for finite clusters with open boundary conditions (●).

To calculate β we used finite clusters of the quasiperiodic structure with open boundary conditions. In this way we are not restricted to the few sample sizes which can be realized (see table 1) by the periodic approximants. In figure 7 the proportionality (3) is shown for the eigenstate of lowest eigenenergy in the PL as an example. This state has a significantly larger participation number than all of the other states. A state with the same behaviour has been observed for the AKL (compare figure 6). Due to its extreme behaviour, we have investigated the scaling of this state separately. Figure 7 demonstrates how well the scaling (3) is obeyed and it also confirms that the results do not depend on the boundary conditions,

nor do they depend on the use of finite clusters instead of the periodic approximants: the absolute values of P change slightly, but the exponent β, i.e. the steepness of the lines in figure 7, does not change. For the subsequent analysis typically 36 different samples in 2D and 25 in 3D with $N \in [400, 4000]$ have been evaluated, so a good fit of equation (3) to the data was possible. The resulting values of β for the eigenstates in the 2D PL and the 3D AKL are shown in figures 8 and 9, respectively. The vertical error bars are due to the standard deviation of a mean least-squares fit. The horizontal bars indicate the energy interval from which the respective eigenstates were evaluated. Except for the eigenfunction at the extreme energy presented in figure 7, a computation of the scaling exponents β for individual eigenstates is numerically not possible from our data due to the statistical fluctuations. Such a computation would require significantly larger samples. However, figure 6 has demonstrated that the participation numbers of the eigenstates in small energy intervals do not differ significantly in most cases, so the derived scaling exponents can reasonably be expected to be representative.

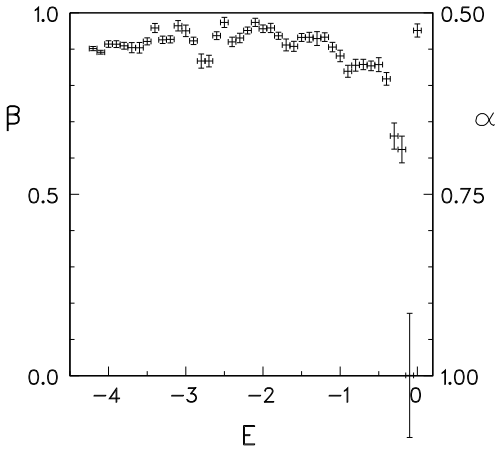

Figure 8. The exponent β for the scaling of the participation number in equation (3) as a function of the energy E for the eigenstates of the PL with open boundary conditions. The right-hand scale gives the exponent α of the power-law decay of the wave functions according to equation (5). The participation numbers have been averaged over an energy interval $\Delta E = 0.1$ for 36 systems with $400 < N < 4000$.

Our calculations show that the localization properties of the eigenstates in 2D are different to those in the Anderson model. The exponent β in figure 8 indicates the most localized states to be around the centre of the spectrum and not at the band edges. We note that the data point $\beta(0) \approx 0.95$ exactly at the band centre is misleading because it reflects rather extended linear combinations of the degenerate eigenstates in the band centre instead of the confined eigenstates themselves. Except for the strongly localized states near the band centre the participation numbers for most of the remaining states show a power $\beta \approx 0.9$, so these states can neither be labelled uniformly extended nor strongly localized. In the following section, larger samples have been analysed to determine whether these states display multifractal, i.e. self-similar behaviour.

On the other hand, the exponent β for the eigenstates of the 3D AKL in figure 9 shows a behaviour similar to the Anderson model. The states at the band edges are more strongly localized than the remaining states around the band centre, which have $\beta \approx 1$ like extended states. We mention that the system sizes of the AKL with $N \leqslant 4000$ are small compared

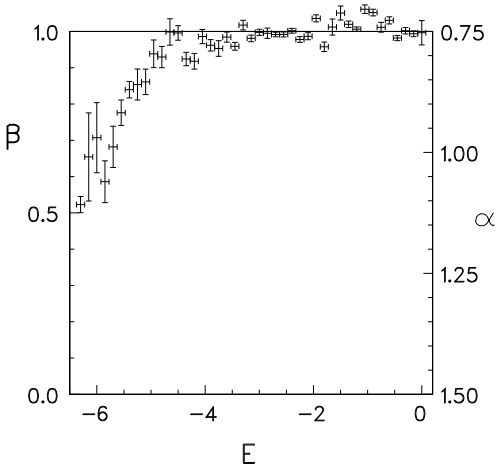

Figure 9. The exponent β for the scaling of the participation number in equation (3) as a function of the energy E for the eigenstates of the AKL with open boundary conditions. The right-hand scale gives the exponent α of the power-law decay of the wave functions according to equation (5). The participation numbers have been averaged over an energy interval $\Delta E = 0.15$ for 25 systems with $400 < N < 4000$.

to the 2D case. A power-law localization for these extended states cannot be concluded. The multifractal analysis of the eigenstates for periodic approximants up to (21, 13) of the AKL in the following section also shows a reduced localization of the states at the band edges and a barely visible multifractal structure of the wave functions.

4.2. Structural entropy

Besides the participation number P or the participation ratio $p = P/N$ we will use the Shannon or information entropy [23, 24] as a characteristic quantity for the description of the localization:

$$S = -\sum_{n=1}^{N} |\psi_{nj}(x)|^2 \ln|\psi_{nj}(x)|^2. \tag{6}$$

The Shannon entropy can be interpreted as a sum of two physical terms [23]: the extension entropy $S_{\text{ext}} = \ln P$, and the deviation from this value which one may call the structural entropy

$$S_{\text{str}} = S - \ln P. \tag{7}$$

While the extension entropy reflects the spatial extent of an eigenstate, because the participation ratio p is a measure of the spatial portion of the system to which a wave function extends, the structural entropy S_{str} contributes an additional amount of information entropy characterizing the shape and thus the structural properties of the distribution of the wave function. It has been shown [23] that the allowed ranges for p and S_{str} are $0 \leqslant p \leqslant 1$ and $0 \leqslant S_{\text{str}} \leqslant -\ln p$. Both quantities, p and S_{str}, are completely determined by a given decay form of the wave function. A further result [23] is that a wave function composed of several identical (or not considerably different) substructures or peaks yields the same (p, S_{str}) values as one composed of a single substructure alone. Plotting the (p, S_{str}) curves calculated for various decay forms in a localization diagram and comparing them with the

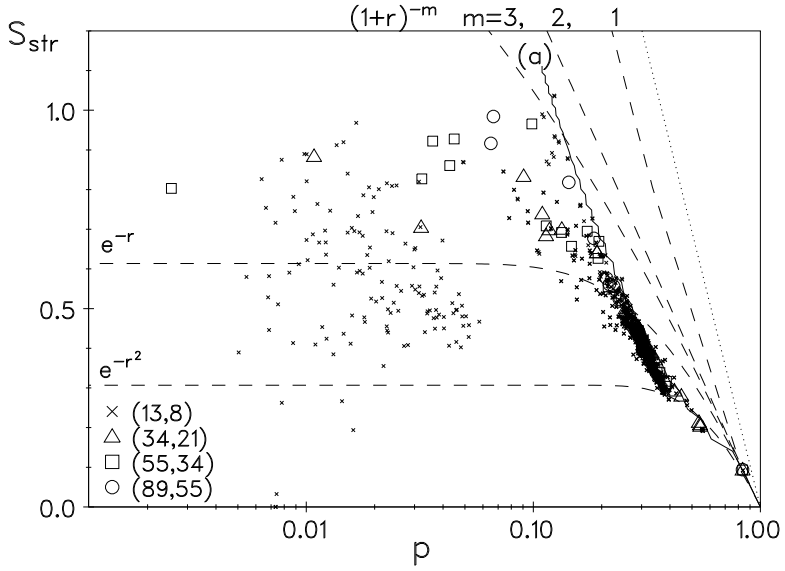

Figure 10. The structural entropy S_{str} versus the participation ratio p for various periodic approximants of the PL with $W = 10^{-5}$ (symbols), compared with the respective dependences (dashed lines) for wave functions of different shape. For the smallest approximant (×) all of the eigenstates have been included in the plot; for the larger approximants only some representative states have been computed. The dotted line reflects the boundary $S_{str} = -\ln p$ of allowed values. The full line is given by equation (8).

values obtained for a given wave function one may derive conclusions on the shape of the states. However, it is unfortunately not possible to decide with certainty on the suitability of a particular decay form from computed values of (p, S_{str}), because different functional forms of the wave function can yield the same (p, S_{str}).

In figures 10 and 11 we have plotted the structural entropy as a function of the participation ratio for the PL and AKL. One can clearly observe a strong correlation of the values of S_{str} and p. In both cases the observed $S_{str}(p)$ can be fairly well reproduced by a decay function with a short-range exponential and a power-law tail with superimposed oscillations:

$$\rho(r) = |\Psi(r)|^2 = \begin{cases} \exp(-r) & \text{for } r < R_0 \\ A\dfrac{\cos(cr+\phi)+1}{r^{2\alpha}} & \text{for } r \geqslant R_0 \end{cases} \tag{8}$$

with $R_0 = 0.75$, $c = 10$, $\alpha = 0.65$ in 2D and $R_0 = 2.5$, $c = 25$, $\alpha = 0.8$ in 3D (see the full lines in figures 10 and 11). The parameters A and ϕ are determined according to the requirement that $\rho(r)$ and $\mathrm{d}\rho(r)/\mathrm{d}r$ should be continuous at $r = R_0$. In figure 10 the states of the PL with participation ratios $p < 0.05$ cannot be described even approximately by equation (8). These states correspond to the spatially confined states in the band centre which would be exactly degenerate without energetic disorder. The behaviour of these states in the case of small energetic disorder is explained in detail elsewhere [14]. In figure 11 only one data point for $E = 0$ deviates significantly from the rest of the data. This is not surprising in view of the fact that only two degenerate states exist in the band centre for the approximant (5, 3) of the AKL. We note that the exponents α of the power-law tail in equation (8) are somewhat larger than those derived from the participation number, equation

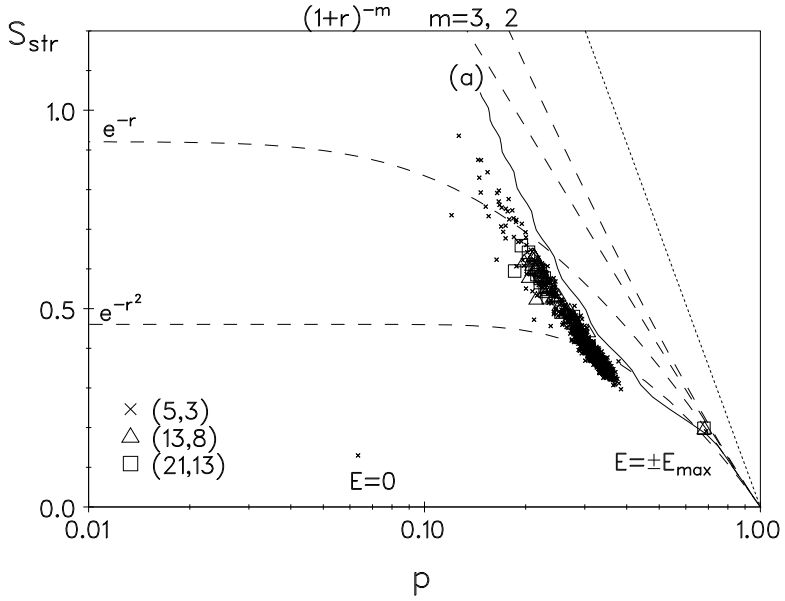

Figure 11. The structural entropy S_{str} versus the participation ratio p for various periodic approximants of the AKL with $W = 10^{-5}$ (symbols), compared with the respective dependences (dashed lines) for wave functions of different shape. For the smallest approximant (×) all of the eigenstates have been included in the plot; for the larger approximants only some representative states have been computed. The dotted line reflects the boundary $S_{str} = -\ln p$ of allowed values. The full line is given by equation (8).

(5). This means that the analysis of the Shannon entropy suggests a stronger localization. However, it must be pointed out that the data points in figures 10 and 11 may be better reproduced by some other decay, different from equation (8), although we did not find any better functional form. But therefore one should not place too much reliance on power law (8).

5. Multifractal analysis

The multifractal behaviour of wave functions can be comprehensively characterized by the singularity spectrum, which is commonly used to describe multifractal entities [25]. For the computation of the singularity spectrum we use the standard box-counting method [25–27]. First we divide the system with N sites into $N_\delta = \delta^{-D}$ boxes B_k of linear size δ, the ratio of the box size and the system size. The probability of finding an electron in the kth box B_k is given by $\mu_k(\delta) = \sum_{n\in B_k} |\psi_{nj}|^2$ for $k = 1, \ldots, N_\delta$. The normalized qth moment of this probability

$$\mu_k(q,\delta) = \mu_k^q(\delta) \Big/ \left(\sum_{l=1}^{N_\delta} \mu_l^q(\delta) \right)$$

constitutes a measure. From this probability measure one obtains the Lipschitz–Hölder exponent or singularity strength α and the corresponding fractal dimension f of an

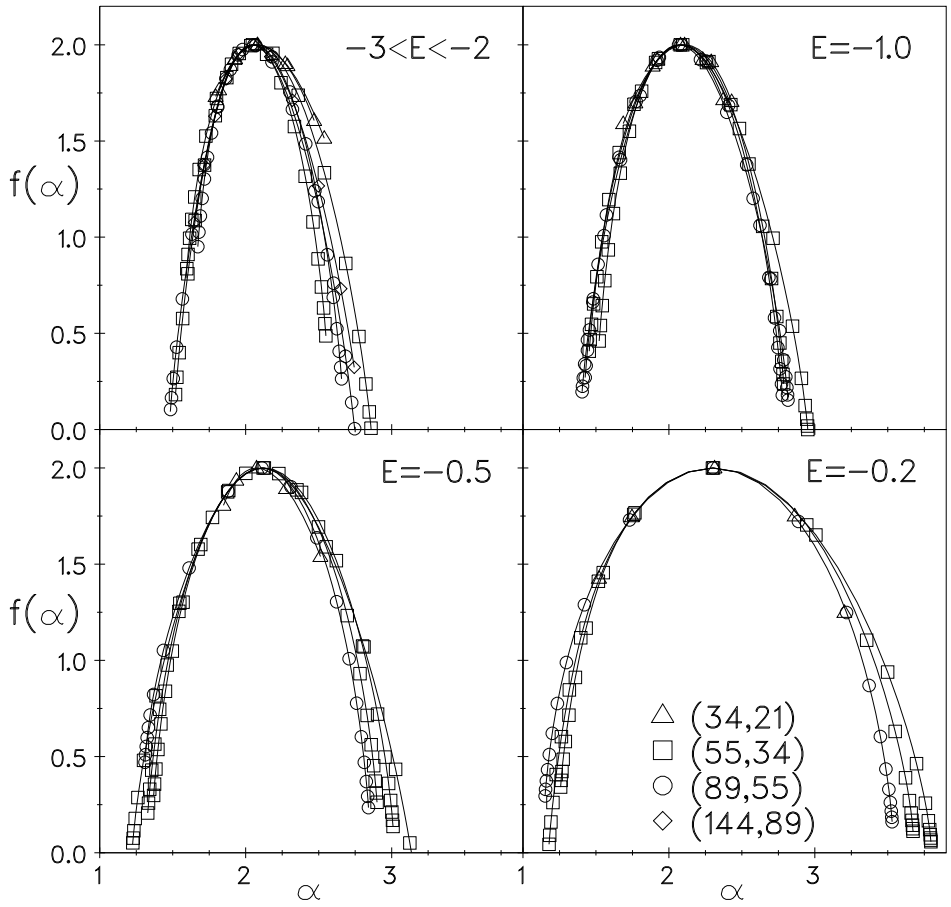

Figure 12. Singularity spectra for various eigenstates in periodic approximants of the PL with $W = 10^{-5}$ at different energies E. The symbols indicate $\alpha(q)$ and $f(q)$ for integer values of q in the parametric representation, equation (9).

eigenstate:

$$\begin{aligned} \alpha(q) &= \lim_{\delta\to 0}\left[\left(\sum_{k=1}^{N_\delta}\mu_k(q,\delta)\ln\mu_k(1,\delta)\right)\Big/\ln\delta\right] \\ f(q) &= \lim_{\delta\to 0}\left[\left(\sum_{k=1}^{N_\delta}\mu_k(q,\delta)\ln\mu_k(q,\delta)\right)\Big/\ln\delta\right] \end{aligned} \tag{9}$$

which yields the characteristic singularity spectrum $f(\alpha)$ in a parametric representation. Hereby, the singularity strength of a box k is defined by $\mu_k \propto \delta^{\alpha_k}$, and the subset of all boxes with the same α forms a fractal set with the number of these boxes $N(\alpha) \propto \delta^{-f(\alpha)}$. It is by no means obvious that the data fulfil equation (9). We have carefully checked that $\sum_k \mu_k \ln\mu_k$ depends linearly on $\ln\delta$ and determined α and f by linear regression. From these results one can also obtain the generalized dimensions

$$D(q) = \frac{f(q) - q\alpha(q)}{1-q}. \tag{10}$$

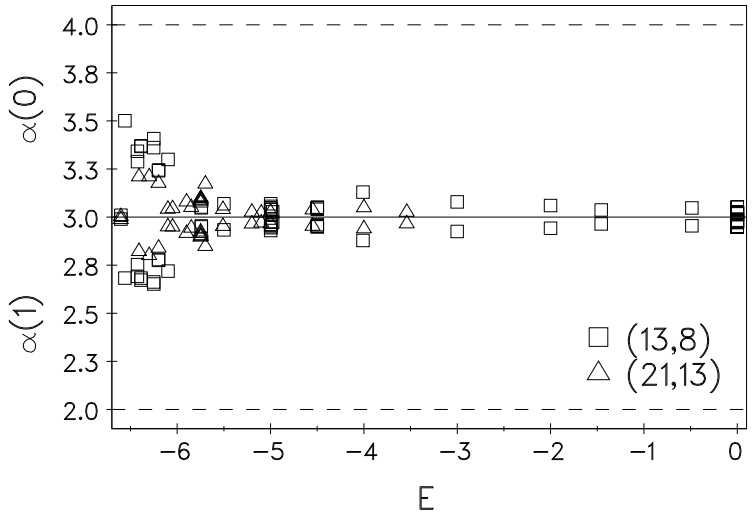

Figure 13. The dependence of the behaviour of $\alpha(0)$ and $\alpha(1)$ for various eigenstates in periodic approximants of the AKL ($W = 10^{-5}$) on the energy E. For all energies, $\alpha(0) \geqslant 3$ and $\alpha(1) \leqslant 3$.

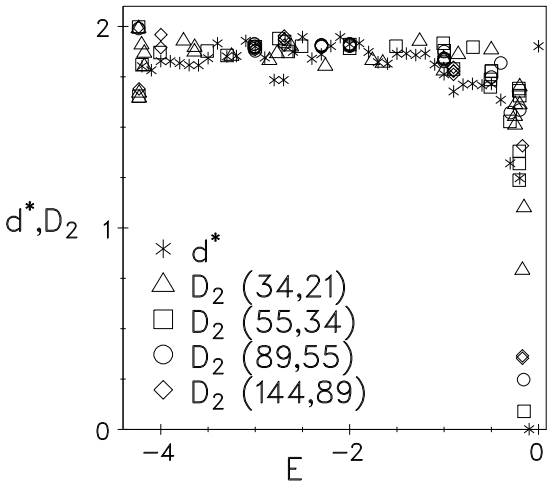

Figure 14. The fractal dimension $d^* = \beta D$ calculated from figure 8 and the correlation dimension $D(2)$ for the eigenstates in periodic approximants of the PL with $W = 10^{-5}$ as a function of the energy E.

We note that $D(1) = \alpha(1) = f(1)$ denotes the information dimension and reflects the scaling of the Shannon entropy (6). The results of the multifractal analysis, namely the singularity spectra of the eigenstates for different approximants of the PL and various energies, are presented in figure 12. Two characteristic values, $\alpha(0)$ and $\alpha(1)$, are shown as a function of the energy for the eigenstates of the approximants of an AKL in figure 13.

The observed independence of the singularity spectra from the system size in figure 12 is an indication that the approximants of the PL used are big enough to avoid finite-size effects. According to the results of Naumis *et al* [9] the eigenstates should show an increasingly

strong multifractal behaviour on changing the energy from the band edges to the band centre. This is corroborated in figure 12, where the singularity spectra become wider with increasing energy.

The dashed lines in figure 13 correspond to the critical values of $\alpha_c(0) = 4$ and $\alpha_c(1) = 2$ at the metal–insulator transition in the 3D Anderson model of localization [28], i.e. they can be used to distinguish extended and localized states. Obviously the AKL states show the behaviour of extended states, and the observed close vicinity of the data to $\alpha(0) = \alpha(1) = 3$ prevents us from proposing a significant multifractal structure of the wave function.

For multifractal wave functions the correlation dimension $D(2)$ can be related [19] to the fractal dimension d^* of the participation ratio given by the exponent β in equation (3):

$$d^* = D\beta. \tag{11}$$

In figures 14 and 15 the fractal dimension calculated from the values of figures 8 and 9 is compared with the correlation dimension for various eigenstates of the 2D PL and the 3D AKL. While in the case of the PL there is a very good agreement of the two dimensions for all energies, in the case of the AKL the agreement is good only for $|E| < 5$, indicating extended states, while the correlation dimension $D(2)$ is much bigger than the fractal dimension d^* for all states with energy $E < -5$. This is clearly an effect of the comparable small systems ($N < 4000$) for the calculation of β in figure 9. As mentioned above, the numerical multifractal analysis shows no indication for multifractal eigenstates in the AKL for any energy.

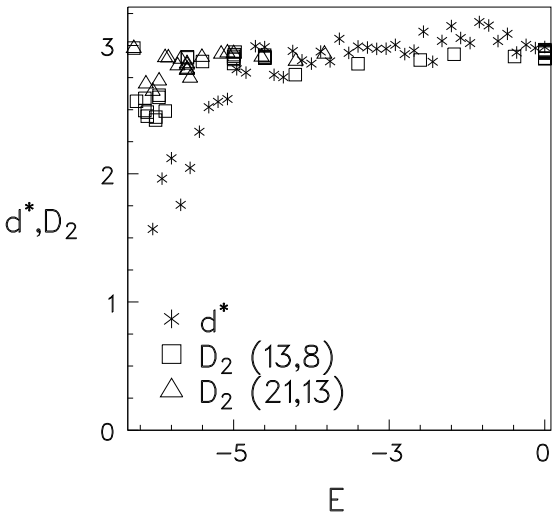

Figure 15. The fractal dimension $d^* = \beta D$ calculated from figure 9 and the correlation dimension $D(2)$ for the eigenstates in periodic approximants of the AKL with $W = 10^{-5}$ as a function of the energy E.

6. Concluding remarks

In this paper a detailed numerical examination of the wave functions in the vertex model of two- and three-dimensional quasiperiodic lattices was presented. We used the dependence of the participation number on the system size and the structural entropy as a function of the

participation ratio to describe the spatial decay of the wave functions and detected a power-law tail with superimposed strong oscillations. With a standard box-counting method we analysed the multifractal properties of the wave functions. In the PL most eigenstates, except the spatially confined states in the band centre, show a power-law localization and a distinct multifractal behaviour depending on the energy. In the AKL a power-law decay of the shape of the wave functions cannot be concluded from the analysis of the participation number, and the eigenstates show no visible multifractal properties. Comparing the results for the exponent β in equation (3) and the correlation dimension $D(2)$, there is no indication that the lattices investigated are still too small to find a marked power-law decay or a multifractal structure. However, due to normalization constraints on the wave functions, a power law with a weaker decay than given by the exponent $\alpha = D/4$ cannot be detected by analysing the participation number or the Shannon entropy. Therefore we can still not exclude the possibility of a weak power-law localization of the eigenstates of the AKL. Our results suggest a tendency towards localization in the tails of the DOS, where we have observed distinct gaps in the spectrum, which may be interpreted as an indication of critical states.

Acknowledgments

Financial support from the Deutsche Forschungsgemeinschaft is gratefully acknowledged. We thank U Grimm for discussions and programming help.

References

[1] Kohmoto M, Sutherland B and Tang C 1987 *Phys. Rev.* B **35** 1020
[2] Fujiwara T, Kohmoto M and Tokohiro T 1989 *Phys. Rev.* B **40** 7413
[3] Penrose R 1974 *Bull. Inst. Math. Appl.* **10** 266
Gardener M 1977 *Sci. Am.* **236** (1) 110
[4] Katz A and Duneau M 1985 *Phys. Rev. Lett.* **54** 2688
Katz A and Duneau M 1986 *J. Physique* **47** 181
[5] Tsunetsugu H, Fujiwara T, Ueda K and Tokihiro T 1991 *Phys. Rev.* B **38** 8879
[6] Sire C 1994 *Lectures on Quasicrystals* ed F Hippert and D Gratias (Les Ulis: Les Editions de Physique) p 505
[7] Tsunetsugu H, Fujiwara T, Ueda K and Tokihiro T 1986 *J. Phys. Soc. Japan* **55** 1420
[8] Tsunetsugu H and Ueda K 1991 *Phys. Rev.* B **43** 8892
[9] Naumis G, Barrio R and Wang C 1994 *Phys. Rev.* B **50** 9834
[10] Rieth T and Schreiber M 1995 *Quasicrystals* ed C Janot and R Mosseri (Singapore: World Scientific) p 514
[11] Kohmoto M and Sutherland B 1986 *Phys. Rev. Lett.* **56** 2740
[12] Fujiwara T, Arai M, Tokohiro T and Kohmoto M 1988 *Phys. Rev.* B **37** 2797
[13] Arai M, Tokohiro T, Fujiwara T and Kohmoto M 1988 *Phys. Rev.* B **38** 1621
[14] Rieth T and Schreiber M 1995 *Phys. Rev.* B **51** 15 827
[15] Krajčí M and Fujiwara T 1988 *Phys. Rev.* B **38** 12 903
[16] Tokohiro T, Fujiwara T and Arai M 1988 *Phys. Rev.* B **38** 5981
[17] Sutherland B 1986 *Phys. Rev.* B **34** 3904
Sutherland B 1987 *Phys. Rev.* B **35** 9529
[18] Schreiber M 1985 *J. Phys. C: Solid State Phys.* **18** 2493
[19] Schreiber M 1985 *Phys. Rev.* B **31** 6146
[20] de Bruijn N G 1981 *Indag. Math.* A **43** 39
Fujiwara T 1990 *J. Non-Cryst. Solids* **117+118** 844
[21] Rieth T and Schreiber M 1997 *Z. Phys.* B **104** 99
[22] Cullum J K and Willoughby R A 1985 *Lanczos Algorithms for Large Symmetric Eigenvalue Computations* vol 1 (Basel: Birkhäuser)
[23] Pipek J and Varga I 1990 *Phys. Rev.* B **42** 5335
Pipek J and Varga I 1992 *Phys. Rev.* B **46** 4978
Pipek J and Varga I 1992 *Phys. Rev.* A **46** 3148

[24] Varga I, Hofstetter E, Schreiber M and Pipek J 1995 *Phys. Rev.* B **52** 7783
[25] Chhabra A and Jensen R 1989 *Phys. Rev. Lett.* **62** 1327
Hentschel H and Procaccia I 1983 *Physica* D **8** 435
Halsey T, Jensen M, Kadanoff L, Procaccia I and Shraiman B 1986 *Phys. Rev.* A **33** 1141
[26] Evertsz C and Mandelbrot B 1992 *Chaos and Fractals* ed H Peitgen, H Jürgens and D Saupe (Heidelberg: Springer) appendix B
[27] Schreiber M and Grussbach H 1991 *Phys. Rev. Lett.* **67** 607
Schreiber M and Grussbach H 1992 *Mod. Phys. Lett.* B **6** 851
[28] Grussbach H and Schreiber M 1995 *Phys. Rev.* B **51** 663
[29] Grussbach H and Schreiber M 1992 *Physica* A **191** 394